Electrochemical and Solid-State Letters, **13** (5) K53-K55 (2010)
1099-0062/2010/13(5)/K53/3/$28.00 © The Electrochemical Society

Heteroepitaxial Growth and Faceting of Ge Nanowires on Si(111) by Electron-Beam Evaporation

Emanuele Francesco Pecora,[a] Alessia Irrera,[a,z] Pietro Artoni,[a] Simona Boninelli,[a] Corrado Bongiorno,[b] Corrado Spinella,[b] and Francesco Priolo[a]

[a]*MATIS-IMM-CNR and Dipartimento di Fisica e Astronomia, Università di Catania, 95123 Catania, Italy*
[b]*CNR-IMM, 95121 Catania, Italy*

We demonstrated the heteroepitaxial growth of single-crystal faceted Ge nanowires (NWs) by electron-beam evaporation on top of Si(111) substrates. Despite the non-ultrahigh vacuum growth conditions, scanning electron microscope and transmission electron microscope images show that NWs have specific crystallographic growth directions ([111], [110], and [112]) and that specific surface crystallographic planes ({111} or {110}) correspond to the [110] and [112] growth directions. Moreover, we studied in detail the Ge NWs structural properties. The temperature dependence of the NW length and of the frequency of each crystallographic orientation has been elucidated. Finally, the microscopic growth mechanisms have been investigated.
 [DOI: 10.1149/1.3339677]

Manuscript submitted January 29, 2010; revised manuscript received February 8, 2010. Published March 15, 2010.

One-dimensional structures, such as carbon nanotubes and semiconductor nanowires (NWs), are considered as realistic additions for the ultimate device miniaturization.[1] Germanium is experiencing a renewed interest for future devices due to its higher hole carrier mobility compared to Si. Moreover, Ge has a smaller bandgap, which is desirable for some detector and solar cell applications in which absorption at longer wavelengths is required.

Ge NWs are generally prepared by the chemical vapor deposition (CVD) technique.[2-7] The orientation and surface faceting of NWs prepared by CVD have been studied;[8,9] they represent key features strictly related to the microscopic growth mechanisms and affect both optical and electrical properties. Physical vapor deposition (PVD) is, in principle, the best method to have an accurate control of the growth mechanisms and of the structural properties of the NWs. Nevertheless, there are no works discussing the growth of Ge NWs by PVD. In particular, electron-beam evaporation (EBE) is a quite simple and widespread deposition technique, and it enables high reproducibility and a precise control of nanostructure growth, offering a pathway toward high throughput production under non-ultrahigh vacuum (UHV) conditions.[10] In this article, the preparation of single-crystal faceted Ge NWs heteroepitaxially grown on Si substrates by EBE has been demonstrated, and the structural features as a function of the experimental parameters have been investigated.

Ge NWs were grown on n-type Si(111) substrates. UV oxidation and HF etch were performed to remove any surface contamination and the native oxide layer before loading the samples into the evaporation chamber (base pressure: $1–2 \times 10^{-8}$ mbar) where both gold and germanium were evaporated by focusing an electron beam on high purity gold pellets or germanium ingots. The deposition rate and film thickness were monitored in situ by a calibrated quartz microbalance and checked ex situ by Rutherford backscattering spectrometry (RBS). The current of the electron gun was set to ensure a flux on the substrate of 1.5×10^{14} atoms/cm^2 s for all samples. During deposition, the substrate was resistively heated. First, a 2 nm thick gold layer was evaporated at room temperature on top of the clean samples. After gold deposition, samples were annealed at 700°C for 2 h to induce the continuous layer breaking and the formation of gold clusters (which act as catalysts) on the substrate. Then, the temperature was decreased in the range between 390 and 510°C for Ge evaporation. The evaporated Ge fluence was varied from 0.5 to 2×10^{18} atoms/cm^2. The pressure during the evaporation processes was about 1×10^{-7} mbar. Structural characterization was performed by a field-emission scanning electron microscope (SEM, Zeiss Supra 25) and a 200 kV transmission electron microscope (TEM, JEOL JEM 2010). NW statistical analysis has been obtained by Gatan digital microscope software; the lattice simulations have been performed by CaRIne crystallography software.

Figure 1a shows a typical low magnification SEM image showing Ge NWs having a specific tilt angle with respect to the substrate; each NW family exhibits a well-defined geometrical surface. We analyzed a large amount of SEM images, and, according to the substrate orientation, we simulated all the possible heteroepitaxial growth directions. We compared the simulations with the experimental images and determined that NWs have only three specific crystallographic directions belonging to the [111], [110], or [112] family. We never observed NWs forming random angles with the substrate or belonging to different growth directions. The measured NW mean radius is about 100 ± 40 nm.

The inset of Fig. 1a shows a [111]-oriented NW [which is perpendicular to the (111)-oriented substrate]. It appears cylindrical, and it is not faceted. In contrast, the other crystallographic directions are always faceted. Figure 1b shows a [110]-oriented NW. The strong similarities between the SEM image (left side) and the simulation (right side) show that the [110]-oriented NWs exhibit quadrangular rombohedric shape and all faces are consistent with the {111} planes. Moreover, the upper part of the NW is not flat, but it exhibits {111} planes only. Figure 1c shows the SEM image and the simulation of a [112]-oriented NW. It is rectangular with the lateral faces oriented in an opposite manner: Two faces exhibit the {111} planes, whereas the remaining two are {110}.

The above results are confirmed by a deeper crystallographic investigation of several NWs performed through TEM images. For this purpose, NWs were mechanically scratched from the substrate and placed onto a copper grid covered by an amorphous carbon layer. A bright-field TEM image, showing a portion of a 2 μm long NW with the catalytic Au particle on top, is reported in Fig. 2. The corresponding diffraction pattern (DP) of the selected area (SA) indicated in the figure is reported in the inset, and it refers to a [111] zone axis (ZA). This implies that the exposed surface corresponds to the (111) plane and that the lateral faces correspond to the (110) planes as they are perpendicular to the $[0\bar{1}1]$ direction. The DPs obtained from several regions along the whole length demonstrate the single-crystal structure of the NW. Moreover, they allow us to identify the growth direction of this NW as [211].

Figure 3a shows the frequency as a function of the growth temperature for each growth orientation. For all orientations, no marked dependence on growth temperature has been found. The [110]-oriented NWs are always the most frequent, and they represent about 70% of the total. The [111]-oriented NWs are about 20% of the total number, whereas the [112]-oriented NWs can be observed very rarely in the samples, with their relative frequency being less than 10%. The different frequencies are probably related to the different surface energies of the different orientations. The measured

[z] E-mail: alessia.irrera@ct.infn.it

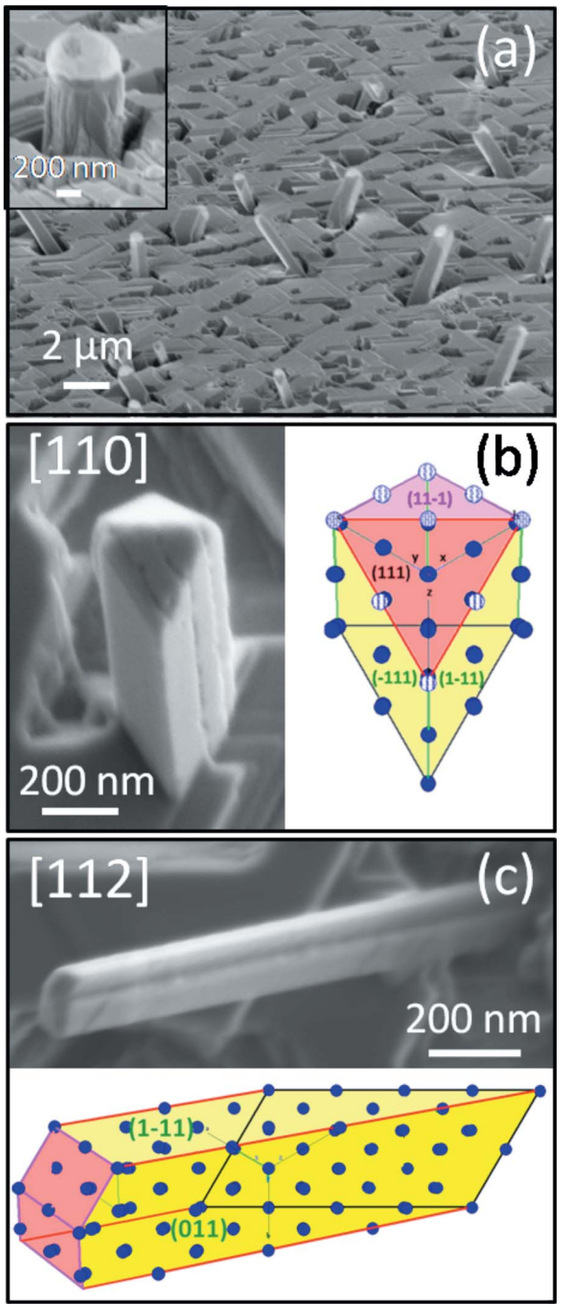

Figure 1. (Color online) (a) Low magnification SEM image of a Ge NWs sample. In the inset, a magnification of a [111]-oriented NW is shown. SEM image and lattice simulation of (b) [110]-oriented Ge NW and (c) [112]-oriented Ge NW. Surface faceting is clearly observed.

areal density of the Ge NWs is about 10^7 cm^{-2}. It is possible to increase the NW density by changing the catalyst preparation. In fact, we have previously demonstrated for Si NWs[11] that by evaporating sequentially gold and Si at the same temperature, the NW density can be increased up to 1 order of magnitude.

Figure 3b shows the NW mean length for a fixed Ge fluence of 1.55×10^{18} cm^{-2} as a function of the growth temperature and for the three orientations. If Ge is evaporated below 380 or above 520°C, no NWs are observable regardless of the orientations. Above 380°C, the NW length increases by increasing the temperature,

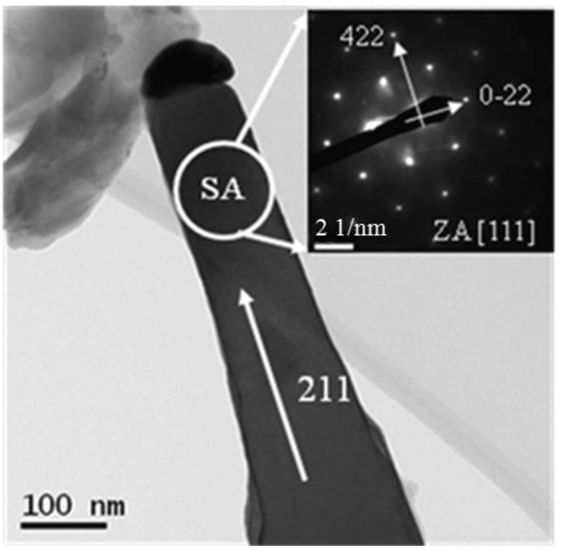

Figure 2. Bright-field TEM image of a [211]-oriented NW. In the inset, the [111] ZA DP relative to the SA indicated by the circle.

reaches a maximum at around 450°C, and then decreases. A similar bell-shaped trend has been found for all orientations.

Figure 4 shows the NW length for each crystallographic orientation as a function of the evaporated Ge fluence for a fixed growth temperature of 450°C. [111]- and [110]-oriented NWs have very similar lengths, ranging from 300 to 1000 nm. The [112]-oriented NWs are always the longest ones, reaching lengths of about 2000 nm. In all cases, the NW length increases by increasing the Ge

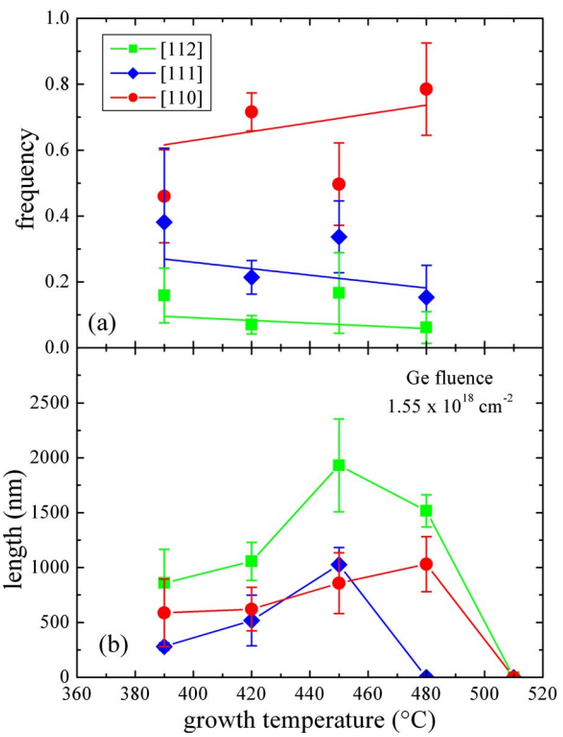

Figure 3. (Color online) (a) NW frequency as a function of the growth temperature for each growth orientation. (b) NW length along the different crystallographic orientation as a function of the growth temperature for a fixed Ge fluence of 1.55×10^{18} cm^{-2}.

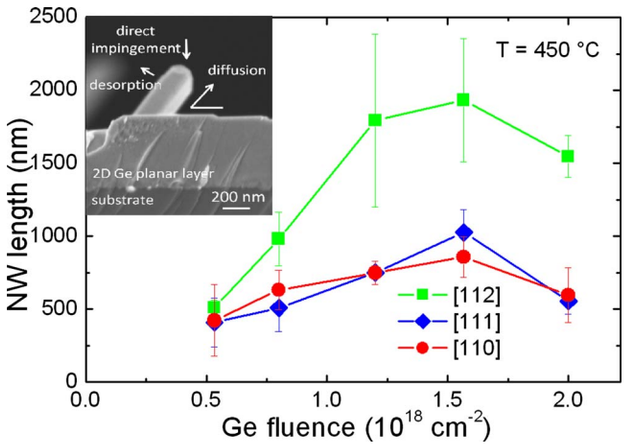

Figure 4. (Color online) NW length for the fixed growth temperature of 450°C as a function of the evaporated fluence for the three different crystallographic orientations. In the inset, a cross-section SEM image showing the substrate, the two-dimensional Ge planar layer, and a NW. The labels indicate the different processes involved during the growth.

fluence up to a maximum value obtained at a fluence of 1.55 $\times 10^{18}$ cm^{-2}. After this value, the NW length does not increase anymore.

Data reported in this article suggest that the microscopic growth mechanisms of heteroepitaxial Ge NWs grown by EBE are similar to the mechanisms previously proposed for Si NWs grown by PVD in the experimental[10,12] and theoretical[13] works. The NW axial growth is the result of a competition with the Ge planar layer growth, as shown in the inset of Fig. 4. Two basic processes are involved during the axial growth: the direct impingement of Ge into the gold droplet and the diffusion and incorporation into the droplets of Ge atoms coming from the substrate. The occurrence of the diffusion and incorporation of Ge atoms into the droplets from the substrate is demonstrated by the presence of a dip around NWs (as shown in Fig. 1); the planar layer around the NW acts as a sort of reservoir for the NW growth. In addition, some Ge atoms can be desorbed, and they would not participate in the growth anymore. We can deduce that by increasing the temperature, we favor the diffusion of Ge atoms deposited on the substrate, and, as a consequence, the axial growth rate increases. In contrast, if the temperature is increased too much (480°C), the detrimental desorption process becomes dominant and the axial rate decreases. Finally, at higher temperatures, the NW growth is totally suppressed.

In conclusion, we have demonstrated that it is possible to grow heteroepitaxial faceted Ge NWs on Si by EBE under non-UHV conditions. NWs have three specific crystallographic orientations ([111], [110], and [112]), and [110] and [112] exhibit a faceted surface with {111} or {110} planes, depending on their orientation. We have shown that the [110] growth direction is the preferred one, whereas the [112]-oriented NWs are the longest ones. Above the eutectic temperature, a narrow temperature window (~100°C wide), in which NWs can be grown, exists, and a bell-shaped temperature dependence of NW growth rate has been found.

Acknowledgments

The authors thank Roberto Lo Savio for the RBS measurements and Carmelo Percolla for the expert technical assistance.

Consiglio Nazionale delle Ricerche assisted in meeting the publication costs of this article.

References

1. http://www.itrs.net, last accessed Mar 8, 2010.
2. A. M. Morales and C. M. Lieber, *Science*, **279**, 208 (1998).
3. J. W. Dailey, J. Taraci, T. Clement, D. J. Smith, J. Drucker, and S. T. Picraux, *J. Appl. Phys.*, **96**, 7556 (2004).
4. T. I. Kamins, X. Li, R. S. Williams, and X. Liu, *Nano Lett.*, **4**, 503 (2004).
5. K. Kang, D. A. Kim, H. Lee, C. Kim, J. Yang, and M. Jo, *Adv. Mater.*, **20**, 4684 (2008).
6. H. Jagannathan, M. Deal, Y. Nishi, J. Woodruff, C. Chidsey, and P. C. McIntyre, *J. Appl. Phys.*, **100**, 024318 (2006).
7. H. Adhikari, A. F. Marshall, C. E. D. Chidsey, and P. C. McIntyre, *Nano Lett.*, **6**, 318 (2006).
8. T. Hanrath and B. A. Korgel, *Small*, **1**, 717 (2005).
9. C. B. Li, K. Usami, T. Muraki, H. Mizuta, and S. Oda, *Appl. Phys. Lett.*, **93**, 041917 (2008).
10. A. Irrera, E. F. Pecora, and F. Priolo, *Nanotechnology*, **20**, 135601 (2009).
11. E. F. Pecora, A. Irrera, and F. Priolo, *Thin Solid Films*, **518**, 2562 (2010).
12. P. Werner, N. D. Zakharov, G. Gerth, L. Schubert, and U. Gösele, *Int. J. Mater. Res.*, **2006**, 1008.
13. V. G. Dubrovskii, N. V. Sibirev, G. E. Cirlin, J. C. Harmand, and V. M. Ustinov, *Phys. Rev. E*, **73**, 021603 (2006).